

In Search of the Weak, Six-Membered Intramolecular Hydrogen Bond in the Solution and Solid States of Guanidinobenzimidazole

Jing Chen,^[a] Peter G. Willis,^[a] Sean Parkin,^[a] and Arthur Cammers*^[a]

Keywords: Hydrogen bond / Conformation / Kinetics / Solvent effects

The chemical literature presents evidence for the nonexistence of the intramolecular hydrogen bond in neutral 2-guanidinobenzimidazole, a result that defies chemical intuition. In the current study, analyses of substituted 2-guanidinobenzimidazoles by dynamic ¹H NMR, IR, and X-ray diffraction unveiled the contribution of the intramolecular hydrogen bond to the overall structure and conformational equilibria. The presence of the intramolecular hydrogen bond in this work and its absence in previous studies of the unsubstituted

parent compound is reconciled by the fact that intramolecular hydrogen bonds between the imidazole moieties and guanidino NH₂ protons were weak. The intramolecular hydrogen bonds were more apparent in derivatives with guanidino NHR. The behavior of the latter indicated competition between and coexistence of inter- and intramolecular hydrogen bonding.

(© Wiley-VCH Verlag GmbH & Co. KGaA, 69451 Weinheim, Germany, 2005)

Introduction

Hydrogen bonding as an argument applies to many fields in the chemical and biological sciences.^[1] Although often invoked in structural descriptions, the impact of intramolecular hydrogen bonds on the energies and conformations of molecules is difficult to quantify.^[2–6] This statement takes on more meaning when the intramolecular hydrogen bond is energetically similar to competing intermolecular interactions; these bonding environments are very different from strong hydrogen bonds.^[7–9] Comparing the molecule under study to an analogue without the intramolecular hydrogen bond should provide the means to measure the bond strength. However, defining the molecule without the intramolecular hydrogen bond is difficult.^[3] In computational studies this issue is less problematic because hydrogen bonds can be defined in terms of atomic contributions.^[10]

Guanidinobenzimidazole (**1**) is a good candidate to study the effect of weak intramolecular hydrogen bonds. The chemical literature supports the *N10*-dehydratautomer of **1** drawn in Figure 1 versus *N12*- or *N13*-dehydratautomers.^[11,12] The intramolecular hydrogen bond, S(6), Etter's notation,^[13] in neutral **1** should be weak because of the non-optimal relative positions of the hydrogen-bond donor guanidine NH and the imidazole hydrogen-bond acceptor.^[14–18]

Examining X-ray crystal structures^[19–22] and performing calculations^[12,23] led to the notion that S(6) in 2-guanidinobenzimidazole **1** should hold all atoms coplanar. Contradic-

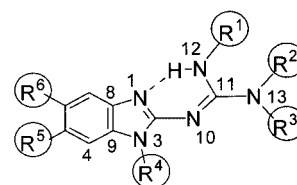


Figure 1. Atom enumeration: **1**: R^{1–6} = H; **2a**: R^{1,3} = *i*Pr, R^{2,4,5,6} = H; **2b**: R^{1,3} = *i*Pr, R^{2,4} = H, R^{5,6} = Cl; **2c**: R^{1,3} = *i*Pr, R² = H, R⁴ = Me, R^{5,6} = Cl; **3a**: R^{2,3} = *i*Pr, R^{1,4,5,6} = H; **3b**: R^{2,3} = *i*Pr, R^{1,4} = H, R^{5,6} = Cl

tory ¹⁵N, ¹³C, and ¹H dynamic nuclear magnetic resonance spectrometry (DNMR)^[9,24–26] studies of **1** found no intramolecular hydrogen bond.^[12,27,28] N12 and N13 exchange rapidly, and the exchange rate between N1 and N3 in **1** at the imidazole ring apparently correlates with the rate of intermolecular exchange of protic ¹H nuclei, because methanol promotes N1/N3 exchange whereas DMSO does not.^[28] Although hydrogen atom exchange of imidazole is usually fast in [D₆]DMSO on the NMR time scale, the rate of exchange varies when imidazole or benzimidazole is substituted at C2.^[29] The S(6) in **1** is absent in 2-aminobenzimidazole, and 2-thiomethylbenzimidazole. However, **1** and the two aforementioned molecules were found to have the same kinetic barriers of tautomerization of the imidazole rings in [D₇]DMF.^[27] Similar temperature dependences of the imidazole NH ¹H chemical shifts of **1** and 2-aminobenzimidazole also indicate a weak or absent intramolecular hydrogen bond in **1** ($\Delta\delta/\Delta T$: -2.1 and -2.8 ppb/K, respectively).^[27]

These issues are reopened in the current study. X-ray diffraction, computation, infrared spectrometry, and ¹H DNMR techniques were applied to derivatives of **1** to

^[a] University of Kentucky, Department of Chemistry, Lexington, Kentucky 40506–0055, USA
Fax: (internat.) +1-859-323-1069
E-mail: a.cammers@uky.edu

characterize the intramolecular hydrogen bond and to appreciate its subtle role in the dynamic conformation and molecular properties of **1**.

Results and Discussion

This study began with non-chlorinated derivatives **2a** and **3a**. The chlorine was included in **2b** and **3b** to define kinetic barriers more accurately by DNMR spectroscopy. A pair of aromatic singlets is easier to model than an ABCD splitting pattern in the regime of slow N1/N3 exchange. Qualitatively, the DNMR behaviors of **2a** and **2b**; and **3a** and **3b** were indistinguishable. We were also more comfortable in drawing conclusions from the solid-state studies with the structural redundancy provided by the chlorinated and non-chlorinated derivatives.

Solid-State Studies

The tape motif is a favored solid-state arrangement of hydrogen bonds in molecules possessing the imidazole moiety.^[30] This motif connects atoms N1 and N3 by intermolecular hydrogen bonds in a structurally diverse set of imidazole derivatives.^[30] However, in the derivatives of **1** studied in this work, some of the N1/N3 intermolecular hydrogen bonds were sacrificed in the solid states to allow for the N1/N12 S(6). In the solid state, derivatives **3** sacrificed the intermolecular hydrogen bond to preferentially establish S(6); derivatives **2** bifurcated the S(6) with the imidazole intermolecular hydrogen bond.

The subtle dependence of the S(6) on competing intermolecular hydrogen bonding is made evident by the solid states of **2b**, **2c** and **3b**, presented as stereo structures in Figure 2. *N,N'*-substituted **2b** possessed the infinite tape hydrogen bonding motif.^[30] The guanidino NH hydrogen-bond donor in the S(6) of **2b** bifurcated the intermolecular hydrogen bond of the tape motif. When the methyl group capped N1 in **2c**, as in *N*¹-methyl-2-guanidinobenzimidazole,^[12] the intramolecular hydrogen bond was established with all atoms coplanar in the solid state. *N,N*-substituted **3b** had four symmetry-unrelated structures. Three of these possessed the intramolecular hydrogen bond as in **2c**. In the fourth symmetry-unrelated molecule of the solid state of **3b**, an intermolecular imidazole NH hydrogen-bond donor broke the intramolecular hydrogen bond.

The chlorine atoms in **2b** and **3b** did not greatly impact hydrogen bonding. The X-ray structure of **2a** had the tape structure analogous to **2b**. Likewise, **3a** (only one symmetry-unrelated molecule) in the solid state was coplanar with S(6) intact, analogous to three out of four of the symmetry-unrelated molecules in the solid state of **3b**. In summary, S(6) appears to compete with the intermolecular hydrogen bonds to a greater extent in *N,N* derivatives **3** than *N,N'* derivatives **2**. A relatively stable S(6) in **3** or relatively weak intermolecular hydrogen bonding in **3** could explain these solid states.

IR studies of derivatives of **1** revealed much similarity between solid- and solution-state distributions of conform-

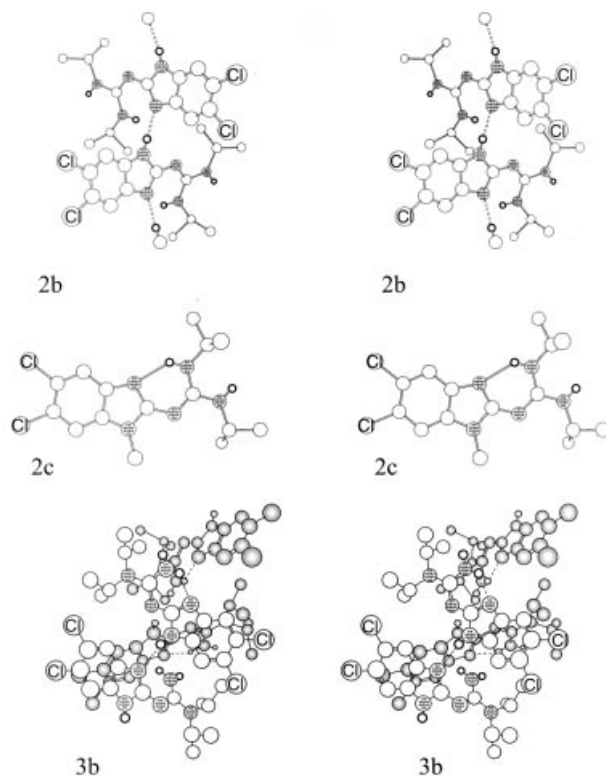


Figure 2. Stereoviews of solid states of **2b**, **2c**, and **3b** are shown above; structure **2b** has the tape hydrogen bond motif with a bifurcated S(6); structure **2c** has the intramolecular hydrogen bond intact; four symmetry-unrelated molecules in the solid state of **3b** have three intramolecular hydrogen bonds intact and one broken by contact with the N1 hydrogen-bond donor of a nearest neighbor; Cl atoms are labeled, and N atoms are hatched; for clarity, the CH protons are omitted, and structure **3b** is depth-cued

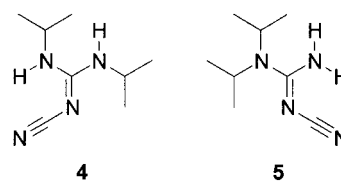


Figure 3. Molecules **4** and **5** were starting materials for the syntheses of structural families **2** and **3**. Molecule **4** was also used as a structural analogue of **2** in ¹H DNMR studies

ers because material dispersed in solid KBr and CS₂ solutions of **2b**, **2c** and **3b** had virtually indistinguishable NH bands. The stretching modes corresponding to N12–H were sharp in both media whereas the stretching modes corresponding to N3–H and N13–H were broad. The alkane region in the IR spectra of solid KBr samples of **2b**, **2c**, **3b**, **4** and **5** were similar. In Figure 4 experimental and computed (rhf/6–311 g) IR spectra were referenced internally at the most intense point of the alkane region, band a. The computed bands (c bands in Figure 4) for the NH hydrogen-bond donors at N3 and N13 did not correspond to the experimental values presumably because of intermolecular hydrogen bonding. However, in **2b**, **2c**, and **3b** the experimental band (b bands in Figure 4) corresponding to the

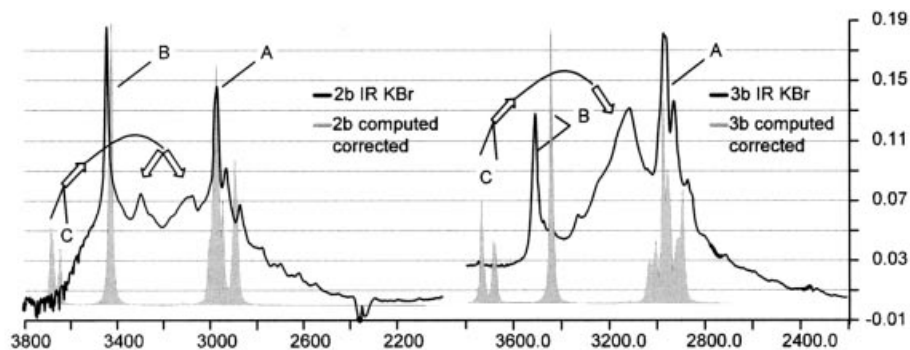


Figure 4. The experimental IR spectra (KBr, dilute) of **2b** (left) and **3b** (right) were compared with computed spectra (gray shadow) (rhf/6–311 g). The calculated spectra were referenced to the experimental spectra at the tallest absorbance in regions A, the alkane stretching. Bands B corresponded to the N12–H stretch of S(6). In **2b**, **2c** and **3b**, its calculated shape and wavenumber corresponded well with the experimental spectra. Regions C are the calculated gas phase guanidino NH hydrogen-bond stretches (3679, 3729 cm^{-1} for **2b** and **3b**, respectively) and the N3–H stretching bands (3647, 3680 cm^{-1} for **2b** and **3b**, respectively). These bands correspond to the broadened and shifted bands in the experimental spectra between 3350–3050 cm^{-1} .

stretching of the guanidino N–H group of S(6) approximated the calculated wavenumbers in value and morphology after they were referenced to the experimental alkane region. This was strong evidence for protection of this N–H group from intermolecular hydrogen-bond acceptors. The bands in the NH regions of the IR spectra of **2b**, **2c**, **3b**, **4** and **5** shifted from 3350–3050 cm^{-1} to 2500–2200 cm^{-1} after D/H exchange (not shown in the figure) upon warming the material for hours in MeOD^[31] followed by recrystallization, thereby confirming their protic nature.

Extrapolating solid-state behavior to solution-state behavior is tenuous, but if a relationship exists in this case, a few hypotheses can be proposed. 1) The intramolecular hydrogen bond in **2c** should be more stable than the one in **2b**, because in **2c** the intermolecular hydrogen bond should compete less with the S(6). Likewise, the S(6) in **2b** should stabilize with dilution in noncompetitive solvents because of less intermolecular competition. 2) The exchange of the *i*Pr-substituted nitrogen atoms in **4** should be more facile than that in **2b** and **2c**. Compound **4** lacks the intramolecular hydrogen bond but is otherwise structurally analogous to family **2**. 3) S(6) in **3** could be more stable than that in **2** because structural family **3** conserves the S(6). 4) The intermolecular hydrogen bonds in *N,N'* derivatives **2** could be more stable than those in the *N,N* derivatives **3** because the solid states of **2** always conserve the intermolecular hydrogen bonds. The solution-state studies below present evidence regarding these four hypotheses.

Solution-State Studies

The mechanism of the exchanges observed must have been a combination of rotation and hydrogen atom exchange. Even though inversion is promoted as the best mechanism for exchange of substituents on two monosubstituted nitrogen atoms of guanidine and related species,^[32–34] inversion at N10 in **1** would have mechanistically united exchanges N1/N3 and N12/N13; however, they are definitely separate events. In elegant experimentation with **1**, Webb et. al. showed that the N12/N13 exchange could be accelerated over the N1/N3 exchange; this

result would have been impossible for inversion at N10.^[28] Furthermore, the chemical literature has examples of exchange of neutral substituted guanidine derivatives interpreted as rotation.^[33,35,36]

The kinetic barriers to exchange are pertinent to the stability imparted by S(6) because S(6) has to break for the exchanges to occur.^[3] In a hydrogen-bonding medium the transition states of the rotations are not devoid of hydrogen bonds. These two notions immediately offer two methods by which S(6) in derivatives of **1** may be evaluated: 1) by choosing a molecule analogous to **1** but lacking S(6) and comparing the barriers to rotation in noncompetitive solvents and 2) comparing the barriers to rotation of the structural families **2** or **3** in protic versus aprotic solvents.

Downfield chemical shifts and small temperature dependencies are characteristic of intramolecular hydrogen bonding. The S(6) separated the ¹H chemical shifts of N12H and N13H of **2a**, **2b**, and **2c** by approximately 6 ppm at –40 °C in CDCl₃ (Figure 5). In [D₇]DMF from –50 to 0 °C, the N12H–S(6) and N13H chemical shifts of **2b** had temperature dependencies, $\Delta\delta/\Delta T$: -1.10 ± 0.01 and -4.74 ± 0.03 ppb/K, respectively. The corresponding numbers for **2c** in CDCl₃ in the same temperature range were 2.11 ± 0.05 and -1.11 ± 0.08 ppb/K, respectively. In the latter case the two peaks diverged. At 0 °C and above these two peaks converged. These observations and the studies presented above indicated an S(6) in derivatives **2**.

In Figure 5, intermolecular association decreased upon 20 × dilution of **2b** in CDCl₃ from 9.0 to 0.4 mM (spectra 6–3 and 5–2) with concomitant broadening of proton A. Imidazole NH proton A also broadened and moved upfield as temperature increased (spectra 1–6). Guanidino NH proton B was broadened greatly because of exchange with proton E at temperatures above –20 °C.

Isochronous NH and CH methine signals in CDCl₃ made line shape analysis^[37,38] with these peaks unreliable (see Figure 5); however, line shape analysis of the *i*Pr CH₃ ¹H NMR signals allowed determination of the N10C11 rotational barrier, $^{\ddagger}\Delta G = 12.7 \pm 0.3$, 13.0 ± 0.1 , and 13.5 ± 0.2 kcal/mol for **2b** at 8.8 and 0.4 mM and **2c** at 5.7 mM, respectively.

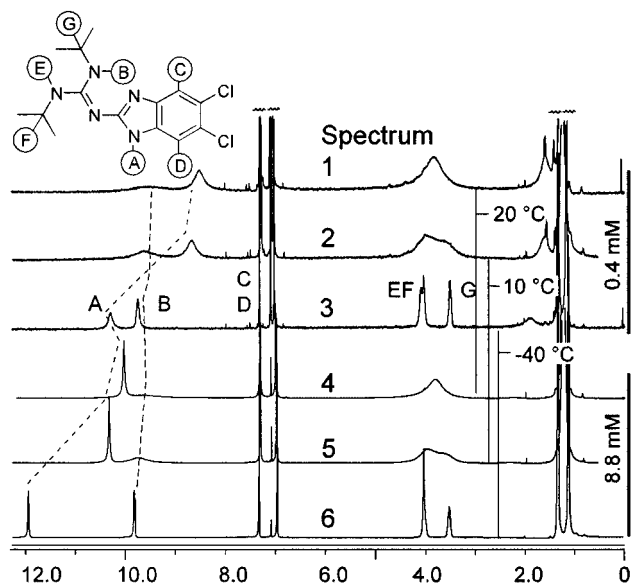


Figure 5. Stacked ^1H NMR spectra of **2b** in CDCl_3 , as a function of concentration (spectra 1–3 are at 0.4 mM, spectra 4–6 are at 8.8 mM) and temperature (20, 10, and -40°C from top to bottom); pertinent proton signals are labeled A–G

Intermolecular hydrogen bonding tends to decrease with decreasing concentration due to its bimolecular nature. Likewise in **2b**, methyl substitution obstructed intermolecular hydrogen bonding. Thus the barrier to rotation about N10C11 increased as intermolecular association decreased, indicating contributions from S(6). For the N10C11 rotation barrier, contributions from steric effects and S(6) should both be important. If the steric parameter alone were important, the N10C11 rotation would have accelerated with decreased intermolecular association.

Line shape analysis of the ^1H NMR signals in $[\text{D}_7]\text{DMF}$ and $[\text{D}_4]\text{MeOD}$ resulted in solvent-dependent rates of bond rotation about N10C11: for **2b**, ΔG^\ddagger for rotation about N10C11 was 13.6 ± 0.6 kcal/mol in $[\text{D}_7]\text{DMF}$ and 11.0 ± 0.5 kcal/mol in $[\text{D}_4]\text{MeOH}$. The solvent-dependence follows the hydrogen bond-dependent trend established above. Hypothetically, the electron-donor solvent, $[\text{D}_7]\text{DMF}$, hydrogen-bonded with the imidazole NH of **2** and did not compete strongly with S(6). However, the hydrogen-bond-donor solvent ($[\text{D}_4]\text{MeOH}$) strongly competed with S(6). The difference between these two values is 2.5 ± 0.5 kcal/mol and serves as an estimate of the stability of S(6) in **2b**.

Another estimate of the stability of S(6) in **2** was available with the comparison of the N10C11 rotation rate in **2b** with the analogous rotation rate in **4** (rate of *i*Pr exchange). Since **4** lacks an intramolecular hydrogen bond, but is otherwise structurally analogous to **2**, this difference in rates can be ascribed to the stability of the intramolecular hydrogen bond. Line shape analysis of the methine signals of **4** gave 11.2 ± 0.1 kcal/mol for the $^\ddagger\Delta G$ for rotation about N10C11. This value differed from the corresponding rotation in **2b** (12.7 ± 0.1 kcal/mol at 8.8 mM and 13.0 ± 0.1 kcal/mol at 0.4 mM) by 1.5, and 1.8 kcal/mol. When compared to the

corresponding rotation in **2c** (13.5 ± 0.2 kcal/mol) the difference is 2.3 kcal/mol. The latter value should best approximate the stability of the intramolecular hydrogen bond in **2**, because the methyl blocks effects due to intermolecular hydrogen bonding. The above arguments quantitatively support qualitative hypotheses 1 and 2 offered at the end of the section entitled Solid-State Studies.

Examination of the substitution patterns in **2** and **3** might lead one to predict that N1 and N3 should have similar exchange rates/mechanisms. This exchange corresponds to rotation/H-exchange about the N10C2 bond and must involve breakage of S(6). However at approximately 9 mM in CDCl_3 the N10C2 rotational/H-exchange barrier of **2** was 5 kcal/mol greater than the corresponding barrier in **3**. This barrier should have been dependent on the concentration of adventitious moisture; however, this result was repeated various times with normal precautions to exclude water. The exchange rates for **3** were measured at -50 and -40°C (10.8 kcal/mol) whereas those of **2** were measured at 45 and 40°C (16.2 kcal/mol). In $[\text{D}_4]\text{MeOH}$ the N10C2 rotational barrier in **2** decreased (11.3 kcal/mol at -40°C) corresponding to the complete destruction of S(6), as discussed above. This result demonstrates again that **2** possessed S(6) whereas **3** did not. This could reflect differences in stability of an NH_2 versus an NHR hydrogen-bond donor or intermolecular access to the hydrogen-bond functions in general. Hypothesis 3, derived from the X-ray data, stated that the S(6) in **3** might be more stable than the S(6) in **2**. These solution-state studies falsify hypothesis 3.

In CDCl_3 the chemical shift of the imidazole proton of molecule **3** changed similarly with temperature and concentration as the analogous proton in **2** (proton A, Figure 5). However, the linewidths at half height of the signal in **2** were 11 and 78 Hz at $-40^\circ\text{C}/8.8$ mM and $20^\circ\text{C}/0.4$ mM, respectively, whereas the corresponding linewidths of **3** were 88 and approximately 798 Hz at the same temperatures and concentrations (not shown). In the assumption that the solid state reflects the solution state, hypothesis 4 (above) posited that molecule **2** should associate more than molecule **3**. The ^1H NMR in a noncompetitive solvent certainly supports this hypothesis.

Conclusion

These physical studies of derivatives of **1** found evidence for a weak intramolecular hydrogen bond between N1 and N12 of **2b** (2.3 ± 0.5 kcal/mol) by two methods. When the intramolecular hydrogen bond in parent molecule **1** was measured against benchmarks dependent on intermolecular interactions such as $\Delta\delta/\Delta T$ and tautomerization rates, no stabilization from the intramolecular hydrogen bond was found.^[27] This work questioned what should be learned from the previous study. For example, can all S(6)-type hydrogen bonds involving nitrogen atoms be dismissed as negligible energetic contributions to molecular conformation? The answer is no. In the current study, the *N,N*-dialkyl derivatives **3** showed little evidence of an intramolecular hy-

drogen bond, whereas the *N,N'*-dialkyl derivatives **2** showed much evidence for a weak intramolecular hydrogen bond. The parent molecule should reasonably behave like the *N,N'*-dialkyl derivatives if the $-\text{NH}_2$ guanidino hydrogen-bond donor is more kinetically labile than the $-\text{NHR}$ guanidino hydrogen-bond donor, as indicated by this work.

Another plausible hypothesis for the stability of the hydrogen bonds finds a basis in solvent-accessible surface area (SASA). Increased stability from buried hydrogen bonds in proteins is a major argument in protein folding.^[39–41] This argument is most often framed in terms of SASA.^[42,43] A large difference between the two substitution patterns, **2** and **3**, was the SASA of the protic groups of the guanidino substituents. The dimers from the crystal structure coordinates are depicted in Figure 6, which shows that the dimer of **2b** effectively hides the SASA associated with its S(6), but **3b** does not. The same conclusion can be reached by considering the electrostatic potential of the SASA of energy-minimized single molecules of **2a** and **3a**. The proton functionality in **3** is made more available by the fact that the N13C11 bond rotates rather freely in **3** because of steric destabilization of the planar conformation, whereas the N13C11 bond in **2** rests in the *all-trans* (*triskelion*) conformer. Interesting steric effects on the nature of S(6) have been reported previously.^[44,45] If this SASA-based rationalization is correct, the S(6) in parent molecule **1** should provide even less stability to the overall structure than derivatives **3** because the proton functionality in **1** is more exposed than that in **3**; this notion is in agreement with the results of the previous study in which no S(6) was detected in **1**.^[27]

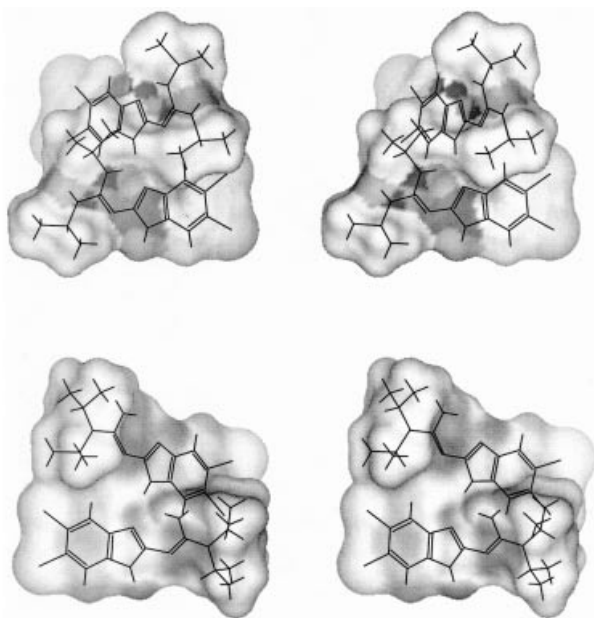


Figure 6. Stereodiagrams of solvent accessible surface (probe radius: 1.5 Å) of the dimers of **2b** (above) and **3b** (below). The diagrams show the electrostatic potential of the VW surface. The guanidino NH is inaccessible to solvent in **2b** but is readily accessible in **3b**. This figure was composed using atomic coordinates from the crystal structures, imported into ViewerLite 5.0, Accelrys Inc. 2002

Should the dashed bond in **1** be drawn in a realistic representation of the behavior of the molecule? This is obviously not a simple answer; it is very humbling that such a simple molecule gives rise to such complex dynamics. Answer: draw the dashed bond, but bear in mind that reality is more complex than the information encoded in the static Lewis structure.

Experimental Section

Physical Studies: The NMR-derived exchange rates were calculated by fitting calculated spectra to experimental spectra by full line shape analysis implemented by gNMR™. Chemical exchange calculations in gNMR use Liouville representations of dynamic spin systems with fitting algorithms described by Binsch.^[38,46] Line width parameters needed for the curve fitting were estimated from residual solvent peaks (approximately 0.5 Hz). The experimental data sets were Fourier transformed and phased under gNMR spectroscopy. In some cases baseline corrections and peak editing were necessary. The rates were determined at more than one temperature near the coalescence region to minimize error.^[37,38] Only cases simple enough to model with a two-states-related-by-one-rate process were determined. For example, there were situations in which H4 and H7 were unequally broadened by a moderate hydrogen-atom exchange at N1; such a situation was deemed beyond the scope of this study. Usually the rates were determined over a range of temperatures to check for linearity in the van't Hoff equation. The energy barriers were calculated by substituting the exchange rate, k , into the Eyring equation, $\ln(k) = \ln(k_B T/h) - \Delta G^\ddagger/RT$. The error in rate measurements near coalescence temperatures was approximately 2%. The concentration of the analyte was carefully controlled, because some rates were dependant on proton availability. Figure 7 shows the results of a full line-shape analysis. The line shape is less than perfect because the residual solvent peak was removed from the experimental spectrum prior to least-squares fitting to a Lorentzian line shape. The $\log(k)$ of the H4/H7 exchange of this spectrum is 1.68 ± 0.04 .

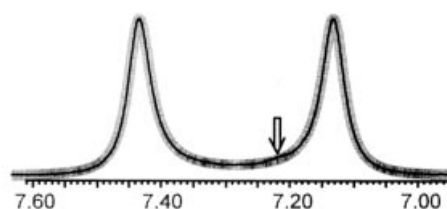


Figure 7. The results of a full line shape analysis of H4 and H7 of **2b** at 45 °C. The calculated spectrum (gray) and experimental spectrum (black) are overlaid; the arrow indicates a region of maximum error where the CHCl_3 solvent peak was edited from the experimental spectrum prior to line-shape fitting

The 5,6-dichlorobenzimidazole derivatives were used instead of the unsubstituted benzimidazole derivatives to simplify the aromatic splitting pattern. The patterns involving two singlets merging to one singlet are much easier to model than ABCD spin systems merging to AA'BB' splitting patterns. Regardless, dynamic spectra deemed too difficult to model were encountered in this study.

IR Studies: IR spectra were collected at room temperature on a Nicolet Magna-IR560 spectrometer. For the solid-state studies, a

sample (1.8 mg) was mortar ground with KBr (100 mg). Part of the mixture was pressed into a thin wafer. For solution-state studies, samples (20 mg) were dissolved in CS₂ (0.5 mL); three drops of solution were placed between two NaCl disks. Deuterium exchange was performed by evaporating CD₃OD (1 mL × 2) from a sample (10 mg). The solids were dissolved in CD₃OD (1 g) and refluxed for 6 h before reduced-pressure evaporation. The exchanged sample (1.8 mg) was mixed with KBr (100 mg) and was pressed wafer-thin.

X-ray Diffraction Studies: X-ray diffraction data were collected at either 90.0(2) K (**2b**, **2c**, **3b**, **4**) or 173(1) K (**2a**, **3a**) on a Nonius Kappa CCD diffractometer with graphite-monochromated Mo-*K*_α X-rays on crystals mounted in paratone oil. Raw data were integrated, scaled, merged and corrected for Lorentz polarization effects with the Denzo-SMN package.^[47] The structures were solved by direct methods using SHELXS-97 and completed by difference Fourier in SHELXL-97.^[48] Structure refinement was carried out against *F*² by weighted full-matrix least-squares in SHELXL-97. Hydrogen atoms were found in difference maps, but were subsequently placed at calculated positions and refined using riding models with isotropic displacement parameters derived from their parent atoms. Non-hydrogen atoms were refined with anisotropic displacement parameters. Atomic scattering factors were taken from the International Tables for Crystallography vol. C.^[49] Crystal data and relevant details of the structure determinations are summarized in Table 1. Structures **2a**, **2c**, **3a** and **4** posed no particular problems although the data for **3a** were weak, resulting in a relatively high *R*-value for such a simple light-atom structure. Structure **3b** was unusual in that it had four independent molecules in the asymmetric unit, but the structure determination was otherwise unremarkable. The determination of **2b** on the other hand was problematic. The crystals, all of which were twinned, contained two molecules per asymmetric unit and had the symmetry of the uncommon space group *P2/n*. Refinement of the twin fraction was performed against a two-component data set (HKL5 format in SHELXL). They diffracted very weakly and required a severe truncation of the high-resolution data to 42° in 2θ. This, in turn, necessitated the use of similarity restraints (SAME in SHELXL) between the two crystallographically nonequivalent molecules, and of rigid-bond (DELU) and approximate-isotropy (ISOR) restraints on the atomic displacement parameters. Despite these problems, the molecular connectivity and packing within crystals of **2b** is unambiguous. Furthermore the molecular associations in **2b** were very similar to those of its structural analogue **2a**. The determination of the atomic coordinates of **2a** were straightforward.

Synthesis: **2-(*N,N'*-diisopropylguanidino)benzimidazole (2a)** was synthesized analogously to **2b**. ¹H NMR (400 MHz; [D₄]MeOH): δ = 7.20 (m, 2 H), 6.95 (m, 2 H), 4.02 (sept, *J* = 6 Hz, 2 H), 1.23 (d, *J* = 7 Hz, 12 H) ppm. ¹³C NMR (100 MHz; [D₄]MeOH): δ = 158.8, 155.2, 137.5, 120.1, 111.9, 42.6, 22.1 ppm. IR (KBr): ν̄ = 3431, 2971, 1598, 1529, 1461, 1402, 1367, 1273, 1176, 736 cm⁻¹. EI-MS: *m/z* = 259 (≈70%), 244 (20%), 159 (100%), 158 (45%), 134 (20%). Single-crystal X-ray diffraction analysis of material crystallized from warm EtOAc confirmed connectivity.

2-(*N,N'*-Diisopropylguanidino)-5,6-dichlorobenzimidazole (2b): *N,N'*-diisopropyl-*N''*-cyanoguanidine (**4**) (606 mg, 3.6 mmol) was added to a solution of 4,5-dichloro-1,2-phenylenediamine (531 mg, 3.0 mmol) in HCl (13 mL, 2 N aqueous solution). The reaction was heated to 90 °C for 21 h. Na₂CO₃ (40 mL, 1 M) was added, and the mixture was extracted with EtOAc (3 × 40 mL) that was washed with brine and dried over MgSO₄. The organic phase was evaporated and purified by flash silica gel chromatography (hexane/

EtOAc, 3:1). Molecule **2b** crystallized from the eluent in 49% yield (484 mg). M.p. 184–186 °C. ¹H NMR (400 MHz, CDCl₃, 20 °C): δ = 10.26 (s, 1 H), 9.90 (br. s, 1), 7.49 (s, 1 H), 7.17 (s, 1 H), 3.92 (br. s, 3 H), 1.30 (br. s, 12 H) ppm. ¹³C NMR (100 MHz, [D₄]MeOH): δ = 160.1, 155.3, 142.7, 131.4, 124.1, 123.0, 117.3, 109.8, 43.4, 23.4 ppm. MS (MALDI): *m/z* = 328 [MH⁺]. Single-crystal X-ray diffraction confirmed connectivity.

1-Methyl-2-(*N,N'*-diisopropylguanidino)-5,6-dichlorobenzimidazole (2c): *N*-(5,6-dichloro-1*H*-benzimidazol-2-yl)-*N',N''*-diisopropylguanidine (**2b**) (328.2 mg, 1.0 mmol), potassium *tert*-butoxide (112.2 mg, 1.0 mmol), and 18-crown-6 (13.2 mg, 0.05 mmol) were dissolved in THF (7 mL) at 0 °C. Methyl iodide (1.0 mmol, 62.2 μL in 2 mL THF) was added dropwise, and the mixture was kept at room temperature for 17 h. The volume of THF was reduced in vacuo, and the mixture was neutralized with NaHCO₃ (1 M). The organic layer was extracted with EtOAc (3 ×) that was washed with brine. The organic phase was evaporated and purified by flash silica gel chromatography (hexane/EtOAc, 3:1) to give **2c** as light-yellow crystals. Yield 44% (0.151 g). M.p. 135–137 °C. ¹H NMR (400 MHz, CDCl₃, 20 °C): δ = 9.77 (s, 1 H), 7.46 (s, 1 H), 7.13 (s, 1 H), 3.97 (b, 3 H), 3.56 (s, 3 H), 1.31 (d, *J* = 6 Hz, 12 H) ppm. ¹³C NMR (100 MHz, [D₆]DMSO): δ = 159.2, 154.4, 141.2, 133.5, 121.9, 120.5, 115.6, 108.8, 42.1, 28.0, 22.8 ppm. MS (MALDI): *m/z* = 342 [MH⁺]. Single-crystal X-ray diffraction analysis of material crystallized from diethyl ether and hexane solution confirmed connectivity.

2-(*N,N*-Diisopropylguanidino)benzimidazole (3a) was synthesized in an analogous manner to **3b**. Material **3a** (232 mg, 0.894 mmol, 71% crude yield) was crystallized from hexane and EtOAc. ¹H NMR (300 MHz; [D₄]MeOH): δ = 7.99 (dd, *J* = 26, 7 Hz, 2 H), 7.61 (dt, *J* = 7, 2 Hz, 2 H), 4.21 (sept, *J* = 6.8 Hz, 2 H), 1.34 (d, *J* = 7 Hz, 12 H) ppm. ¹³C NMR (75.3 MHz; CDCl₃): δ = 156.7, 146.6, 131.3, 129.3, 59.0, 26.5, 22.4 ppm. IR (KBr pellet): ν̄ = 3493.6, 3393.2, 3120.11, 2973.0, 1626.2, 1606.8, 1516.2, 1486.3, 1457.9, 1388.6, 1272.1, 1215.2, 1136.2 cm⁻¹. calcd. C₂₂H₂₁N₅: C 64.84, H 8.16, N 27.00; found C 64.76, H 8.06, N 26.92. Single-crystal X-ray diffraction analysis confirmed connectivity.

2-(*N,N*-Diisopropylguanidino)-5,6-dichlorobenzimidazole (3b) was synthesized in a manner analogous to **2b** except that *N,N*-diisopropyl-*N''*-cyanoguanidine (**5**) (191.4 mg, 1.14 mmol) was used instead of **4**. Yield 59% (0.182 g). M.p. 164–166 °C. ¹H NMR (400 MHz, [D₆]acetone): δ = 10.47 (br. s, 1 H), 7.93 (br. s, 2 H), 7.33 (s, 2 H), 4.21 (sept, *J* = 6.7 Hz, 2 H), 1.30 (d, *J* = 6.7 Hz, 12 H) ppm. ¹³C NMR (100 MHz, [D₆]acetone): δ = 161.3, 157.9, 138.6, 123.0, 113.7, 46.9, 21.3 ppm. MS (MALDI): *m/z* = 328 [MH⁺]. Single-crystal X-ray diffraction analysis of material crystallized from CHCl₃ confirmed connectivity.

***N,N'*-Diisopropyl-*N''*-cyanoguanidine (4):** A mixture of cyanamide (2.0 g, 47.6 mmol) and *N,N'*-diisopropylcarbodiimide (17 mL, 108.6 mmol) was stirred and heated to 110 °C for 15 h. Excess carbodiimide was evaporated under high vacuum. The resulting solid was crystallized in ethanol (70 mL) to give **4** as white crystals. Yield 54% (4.3 g). M.p. 193–195 °C. ¹H NMR (400 MHz, CDCl₃): δ = 4.72 (s, 2 H), 3.81 (m, 2 H), 1.23 (d, *J* = 6.8 Hz, 12 H) ppm. ¹³C NMR (100 MHz, [D₄]MeOH): δ = 159.6, 120.5, 45.1, 22.9 ppm. MS (MALDI): *m/z* = 169 [MH⁺]. Single-crystal X-ray diffraction analysis of material crystallized from EtOH/ CH₃CN confirmed connectivity.

***N,N*-Diisopropyl-*N'*-cyanoguanidine (5):** Concentrated HCl (2.0 mL) was added dropwise to the mixture of sodium dicyan-

Table 1. Crystal data

	molecule 2a	molecule 2b	molecule 2c
formula	C ₁₄ H ₂₁ N ₅	C ₁₄ H ₁₉ Cl ₂ N ₅	C ₁₅ H ₂₁ Cl ₂ N ₅
formula mass	259.36	328.24	342.27
crystal system	monoclinic	monoclinic	monoclinic
space group	<i>P</i> 2 ₁ / <i>c</i>	<i>P</i> 2 ₁ / <i>n</i>	<i>P</i> 2 ₁ / <i>c</i>
<i>a</i> (Å)	8.0810(3)	19.1251(11)	10.1050(4)
<i>b</i> (Å)	21.1140(7)	9.8689(6)	10.6910(4)
<i>c</i> (Å)	9.6270(3)	19.2477(11)	16.0700(7)
<i>a</i> (°)	90	90	90
<i>β</i> (°)	114.2021(14)	113.545(3)	95.777(3)
<i>γ</i> (°)	90	90	90
<i>V</i> (Å ³)	1498.21(9)	3330.4(3)	1727.27(12)
<i>Z</i>	4	8	4
<i>D</i> (calcd.) (Mg/m ³)	1.150	1.309	1.316
<i>T</i> (K)	173(1)	90.0(2)	90.0(2)
crystal size (mm ³)	0.26 × 0.25 × 0.20	0.25 × 0.10 × 0.10	0.40 × 0.38 × 0.32
<i>F</i> (000)	560	1376	720
abs. coeff. (mm ⁻¹)	0.073	0.391	0.380
<i>θ</i> data collection range	1.93–27.49	1.94–21.00	2.28–27.48
reflins. collected	11517	3578	7207
ind. reflns.	3457	3578	3944
data/restraints/parameters	3457/0/177	3578/411/388	3944/0/204
<i>R</i> ₁	0.0497	0.1052	0.0385
<i>R</i> _{all}	0.0784	0.1285	0.0545
goodness of fit on <i>F</i> ²	1.032	1.324	1.056
largest diff (e ⁻ Å ⁻³)	0.294, -0.284	0.506, -0.422	0.290, -0.258

	molecule 3a	molecule 3b	molecule 4
formula	C ₁₄ H ₂₁ N ₅	C ₁₄ H ₁₉ Cl ₂ N ₅	C ₈ H ₁₆ N ₄
formula mass	259.36	328.24	168.25
crystal system	monoclinic	triclinic	monoclinic
space group	<i>P</i> 2 ₁ / <i>n</i>	<i>P</i> $\bar{1}$	<i>P</i> 2 ₁ / <i>c</i>
<i>a</i> (Å)	9.6450(5)	13.7180(2)	9.9030(4)
<i>b</i> (Å)	7.7760(4)	14.1430(2)	8.9600(4)
<i>c</i> (Å)	18.8740(10)	18.2470(3)	12.0710(6)
<i>a</i> (°)	90	81.3460(6)	90
<i>β</i> (°)	95.559(3)	88.3960(7)	101.055(2)
<i>γ</i> (°)	90	69.6790(6)	90
<i>V</i> (Å ³)	1408.88(13)	3280.91(9)	1051.20(8)
<i>Z</i>	4	8	4
<i>D</i> (calcd.) (Mg/m ³)	1.223	1.329	1.063
<i>T</i> (K)	173(1)	90.0(2)	90.0(2)
cryst size (mm ³)	0.28 × 0.24 × 0.12	0.40 × 0.12 × 0.10	0.32 × 0.25 × 0.23
<i>F</i> (000)	560	1376	368
abs. coeff. (mm ⁻¹)	0.077	0.397	0.069
<i>θ</i> data collection range	2.29–25.00	1.55–25.00	0.21–27.42
reflins. collected	9104	21854	7299
data/restraints/parameters	2479/48/176	11552/0/773	2391/0/114
<i>R</i> ₁	0.0678	0.0494	0.0469
<i>R</i> _{all}	0.0872	0.0849	0.0647
goodness of fit on <i>F</i> ²	1.097	1.026	1.040
largest diff (e ⁻ Å ⁻³)	0.294, -0.284	0.506, -0.422	0.290, -0.258

amide (2.2 g, 24.7 mmol) and diisopropylamine (2.4 g, 23.7 mmol) in *n*-butyl alcohol (35 mL). The mixture was refluxed at 90 °C for 28 h. NaOH (20 mL, 2 N) and saturated NaCl_(aq) (30 mL) were added. The resulting solution was extracted with EtOAc (3 × 50 mL). The organic phase was washed with brine (50 mL). The organic phases were evaporated under high vacuum. *N,N*-diisopropylidicyandiamide (**5**) was crystallized from the residue from EtOAc; these crystals were not suitable for diffraction. Yield 19% (0.75 g, 4.5 mmol). M.p. 136–138 °C. ¹H NMR (400 MHz, [D₆]acetone):

δ = 6.15 (s, 2 H), 4.06 (sept, *J* = 7 Hz, 2 H), 1.30 (d, *J* = 7 Hz, 12 H) ppm. ¹³C NMR (100 MHz, [D₆]acetone): δ = 161.0, 118.6, 47.9, 20.9 ppm. MS (MALDI): *m/z* = 169 [MH⁺]. Single-crystal X-ray diffraction analysis of material crystallized from CHCl₃ was interesting due to ten symmetry-unrelated molecules in the unit cell. The details of this crystal will be published elsewhere. CCDC-243202 to -243207 contain the supplementary crystallographic data for this paper. (solid-state coordinates for **2a**, **2b**, **2c**, **3a**, **3b**, and **4**). These data can be obtained free of charge from The

Cambridge Crystallographic Data Centre via www.ccdc.cam.ac.uk/data_request/cif.

Acknowledgments

We thank NSF IGERT, DGE9870691 for a predoctoral fellowship to PGW and NSF, CHE-9702287 for financial support. The beginning stages of this research were funded by NASA-EPSCoR of Kentucky. AC thanks Hans J. Reich for sharing his knowledge of DNMR in the initial stages of this study.

- [1] T. Steiner, *Angew. Chem. Int. Ed.* **2002**, *41*, 48–76.
- [2] P. Lipkowski, A. Koll, A. Karpfen, P. Wolschann, *Chem. Phys. Lett.* **2002**, *360*, 256–263.
- [3] G. Buemi, F. Zuccarello, *J. Mol. Struct. THEOCHEM* **2002**, *581*, 71–85.
- [4] V. Bertolasi, P. Gilli, V. Ferretti, G. Gilli, *Chem. Eur. J.* **1996**, *2*, 925–934.
- [5] P. Gilli, V. Bertolasi, V. Ferretti, G. Gilli, *J. Am. Chem. Soc.* **1994**, *116*, 909–915.
- [6] G. Gilli, P. Gilli, *J. Mol. Struct.* **2000**, *552*, 1.
- [7] J. P. H. Charmant, G. C. Lloyd-Jones, T. M. Peakman, R. L. Woodward, *Eur. J. Org. Chem.* **1999**, 2501–2510.
- [8] P. Hodgson, G. C. Lloyd-Jones, M. Murray, T. M. Peakman, R. L. Woodward, *Chem. Eur. J.* **2000**, *6*, 4451–4460.
- [9] I. G. Shenderovich, P. M. Tolstoy, N. S. Golubev, S. N. Smirnov, G. S. Denisov, H.-H. Limbach, *J. Am. Chem. Soc.* **2003**, *125*, 11710–11720.
- [10] U. Koch, P. L. A. Popelier, *J. Phys. Chem.* **1995**, *99*, 9747–9754.
- [11] E. Grudemann, H. Graubaum, D. Martin, E. Schiewald, *Magn. Reson. Chem.* **1986**, *24*, 21–30.
- [12] C. Acerete, J. Catalan, F. Fabero, M. Sanchez Cabezudo, R. M. Claramunt, J. Elguero, *Heterocycles* **1987**, *26*, 1581–1586.
- [13] M. C. Etter, *Acc. Chem. Res.* **1990**, *23*, 120–126.
- [14] I. Nobeli, S. L. Price, J. P. M. Lommerse, R. Taylor, *J. Comp. Chem.* **1997**, *18*, 2060–2074.
- [15] A. Vedani, J. D. Dunitz, *J. Am. Chem. Soc.* **1985**, *107*, 7653–7658.
- [16] G. Klebe, *J. Mol. Biol.* **1994**, *237*, 212–235.
- [17] J. P. Glusker, *Acta Crystallogr. D* **1995**, *51*, 418–427.
- [18] G. R. Desiraju, *Acc. Chem. Res.* **2002**, *35*, 565–573.
- [19] M. R. Caira, *Top. Curr. Chem.* **1998**, *198*, 163–208.
- [20] P. J. Steel, *J. Heterocycl. Chem.* **1991**, *28*, 1817–1818.
- [21] W. H. Watson, J. Galloy, D. A. Grossie, F. Voegtle, W. M. Mueller, *J. Org. Chem.* **1984**, *49*, 347–353.
- [22] M. R. Caira, W. H. Watson, F. Vögtle, W. Müller, *Acta Crystallogr., Sect. C: Cryst. Struct. Commun.* **1984**, *40*, 1047.
- [23] R. M. Hernández-García, N. Barba-Behrensa, R. Salcedoc, G. Höjer, *J. Mol. Struct. THEOCHEM* **2003**, *637*, 55–72.
- [24] L. M. Jackman, F. A. Cotton in *Dynamic Nuclear Magnetic Resonance Spectroscopy*, Academic Press, New York, NY, **1975**.
- [25] J. D. Roberts, *ABCs of FT NMR*, University Science Books, Sausalito, CA, **1990**.
- [26] H. J. Reich, W. S. Goldenberg, B. Ö. Gudmundsson, A. W. Sanders, K. J. Kulicke, K. Simon, I. A. Guzei, *J. Am. Chem. Soc.* **2001**, *123*, 8067–8079.
- [27] N. Andrade-López, A. Ariza-Castolo, R. Contreras, A. Vázquez-Olmos, N. B. Behrens, H. Tlahuext, *Heteroat. Chem.* **1997**, *8*, 397–410.
- [28] G. R. Bedford, P. J. Taylor, G. A. Webb, *Magn. Reson. Chem.* **1995**, *33*, 383–388.
- [29] E. P. Papadopoulos, U. Hollstein, *Organic Magnetic Resonance* **1982**, *19*, 188–191.
- [30] A. Cammers, S. Parkin, *CrystEngComm* **2004**, *6*, 168–172.
- [31] M. T. Pope in *Isopolyanions and heteropolyanions*, vol. 3 (Eds.: G. Wilkinson, R. D. Gillard, J. A. McCleverty), Pergamon Press, Oxford, **1987**, pp. 1023–1058.
- [32] H. Kessler, D. Leibfritz, *Tetrahedron Lett.* **1970**, 1423–1426.
- [33] T. Asano, H. Furuta, H. J. Hofmann, R. Cimiraglia, Y. Tsuno, M. Fujio, *J. Org. Chem.* **1993**, *58*, 4418–4423.
- [34] P. D. Wildes, J. F. Pacifici, G. Irick, D. G. Whitten, *J. Am. Chem. Soc.* **1971**, *93*, 2004–2008.
- [35] N. P. Marullo, E. H. Wagener, *Tetrahedron Lett.* **1969**, 2555–2558.
- [36] T. Asano, T. Okada, W. G. Herkstroeter, *J. Org. Chem.* **1989**, *54*, 379–383.
- [37] G. Binsch in *The Study of Intramolecular Rate Processes by Dynamic Nuclear Magnetic Resonance*, vol. 3 (Eds.: E. L. Eliel, N. L. Allinger), John Wiley & Sons, New York, **1968**, pp. 97–192.
- [38] G. Binsch, *J. Am. Chem. Soc.* **1969**, *91*, 1304–1309.
- [39] E. R. Goldman, W. Dall'Acqua, B. C. Braden, R. A. Mariuzza, *Biochemistry* **1997**, *36*, 49–56.
- [40] J. K. Myers, T. G. Oas, *Biochemistry* **1999**, *38*, 6761–6768.
- [41] K. L. Maxwell, A. R. Davidson, *Biochemistry* **1998**, *37*, 16172–16182.
- [42] M. L. Connolly, *Science* **1983**, *221*, 709–713.
- [43] A. Becue, N. Meurice, L. Leherte, D. P. Vercauteren, *J. Comp. Chem.* **2004**, *25*, 1117–1126.
- [44] A. Filarowski, T. Glowiake, A. Koll, *J. Mol. Struct.* **1999**, *484*, 75–89.
- [45] W. Schilf, B. Kamienski, T. Dziembowska, *J. Mol. Struct.* **2002**, *602–603*, 41–47.
- [46] D. S. Stephenson, G. Binsch, *J. Magn. Reson.* **1978**, *32*, 145.
- [47] Z. Otwinowski, W. Minor in *Processing of X-ray Diffraction Data Collected in Oscillation Mode*, vol. 276 (Eds.: C. W. J. Carter, R. M. Sweet), Academic Press, San Diego, CA, **1997**, pp. 307–326.
- [48] G. M. Sheldrick in *SHELX97 – Programs for Crystal Structure Solution and Refinement*, University of Göttingen, Germany, **1997**.
- [49] *International Tables for Crystallography, Vol C: Mathematical, Physical and Chemical Tables*, Kluwer Academic Publishers, Holland, **1992**.

Received June 28, 2004